Journal of Materials Science: Materials in Electronics (2019) 30:14547–14553
https://doi.org/10.1007/s10854-019-01826-8

# Effect of nano-sized metallic Au additions at large scale on the phase stability of Bi-2212 ceramics

**Berdan Özkurt**[1]

Received: 1 May 2019 / Accepted: 4 July 2019 / Published online: 8 July 2019


**Abstract**
$Bi_{1.8}Sr_2Au_xCa_{1.1}Cu_{2.1}O_y$ (Bi-2212) polycrystalline ceramics with x = 0.25, 0.3 and 0.35 have been prepared by the solid-state reaction method. XRD results showed the Bi-2212 phase as the major one in all samples, accompanied by metallic Au, and some secondary phases such as $Bi_2CaO_4$. $T_c$ values are very similar for all samples, indicating that the carrier concentration is independent of the amount of Au. Magnetic properties of samples, determined through magnetic hysteresis measurements (*M–H*) performed at both T = 2 and 10 K, showed that samples maintain their diamagnetic characteristics in all cases. In addition, $J_c$ values, calculated from their magnetic hysteresis loops using the Bean's model, showed that addition of metallic Au in high contents leads to an important increase when compared to the samples with low Au content.

## 1 Introduction

Global climate change has created serious dangers such as acid rains, flash floods, hurricanes, and more rapid melting of glaciers over the environment at the present time, showing that urgent precautions should be instantaneously taken. The release of harmful gases occurred by the use of fossil fuels as energy sources should be minimized for a healthier environment.

One of the most important precautions to be taken to maintain the ecological stability of our world is reducing excessive losses in the generation and consumption of energy, providing energy efficiency. It is obvious that superconductors enabling the conduction of large currents without resistance are very important materials also for many technological applications such as maglev system, magnetic field sensor, trapped flux magnet, magnetic bearings, power cables, etc., leading to a more efficient use of energetic resources [1–5]. Bi–Sr–Ca–Cu–O system, with the general formula $Bi_2Sr_2Ca_{n-1}Cu_nO_{4+2n}$, comprises different phases such as 2212 (n = 2) and 2223 (n = 3). This system has been widely studied due to its various advantages such as high electrical conductivity, large-scale synthesis of the desired phases, and high thermal stability range, when compared to other superconductor families [6, 7].

The improvement of electrical properties in Bi-2212 ceramics is normally based on two different approaches. The first one is centered on the preparation conditions, such as pelletization pressure, sintering time, post-annealing temperature, grinding time, melting techniques, etc. [8–13]. The other one is based on adequate chemical substitutions such as Na and Li, or metallic additions (Ag, Au) [9–20]. Those studies clearly point out that substitution or addition of alkaline elements to the BSCCO system produces larger grains due to the formation of a liquid phase at the sintering temperatures. Moreover, addition of metals such as Au and Ag enhances electrical grain connectivity due to their good electrical conductivity and their insolubility in the superconducting phase, appearing between the grains.

On the other hand, it is well known that the main problems of BSCCO superconductors are high anisotropy, weak links between grains and the rapid decrease of critical current density ($J_c$) under high magnetic fields and high temperatures. In spite of all these limitations, it has been shown that $J_c$ values in BSCCO superconductors can reach the order of $1.3 \times 10^3$ A/cm$^2$ at 77 K by both Na substitution and using the laser floating zone (LFZ) technique, which provides good grain orientation [21]. Moreover, the traveling solvent floating zone method leads to $J_c$ values of $2 \times 10^6$ A/cm$^2$ at 20 K [22], and the electrically assisted LFZ reaches $5.8 \times 10^3$ A/cm$^2$ at 77 K [23].

✉ Berdan Özkurt
berdanozkurt@tarsus.edu.tr

[1] Department of Energy Systems Engineering, Faculty of Technology, Tarsus University, 33400 Tarsus, Turkey

Our recent investigation on superconducting properties of $Bi_{1.8}Sr_2Au_xCa_{1.1}Cu_{2.1}O_y$ (x = 0.0, 0.05, 0.1 and 0.2) studying the effect of nano-sized metallic Au addition in low content, showed that the superconducting properties of Bi-2212 phase could be improved due to a better electrical connectivity between the grains [24]. In fact, the Bi–Sr–Ca–Cu–O system has a high thermodynamic stability, implying that it is possible to make different additions or substitutions without drastically affecting the superconducting characteristics of Bi-2212 phase.

In this paper, Bi-2212 ceramics are synthesized through the classical solid state method with the addition of nanosized metallic Au (15 nm) in high concentrations ($0.25 \leq x \leq 0.35$). Their structural and microstructural features have been studied and related to the superconducting properties.

## 2 Experimental procedure

Commercial $Bi_2O_3$ (Panreac, 98 + %), $SrCO_3$ (Panreac, 98 + %), $CaCO_3$ (Panreac, 98.5 + %), CuO (Panreac, 97 + %) and metallic Au (Nanografi Co. Ltd.,15 nm, 99.9 + %) powders were used for the preparation of polycristalline $Bi_{1.8}Sr_2Au_xCa_{1.1}Cu_{2.1}O_y$ samples with x = 0,25, 0.3, and 0.35. They were weighed in the appropriate proportions, mixed, and milled for 2 h in an agate mortar to get a homogeneous mixture. After the milling process, the powders were uniaxially pressed into pellets of 2.9 cm diameter under 375 MPa for 2 h. The pellets were then calcined at 750 °C for 12 h, reground, repressed, and recalcined twice at 820 °C for 24 h to start the formation of the superconducting phase. Detailed information about material preparation processes can be found in previous works [24]. Finally, the prepared samples after all re-sintering, grinding and pressing processes were annealed at 850 °C for 120 h in order to reach a large amount of pure 2212-BSCCO.

Resistivity and magnetic measurements were carried out in a Cryogenic Limited PPMS (from 5 to 300 K) which could reach 2 K in a closed-loop He system. X-ray powder diffraction analyses were performed by using a Rigaku Ultima IV X-ray diffractometer with a constant scan rate (2°/min) in the range 2θ = 3–60°. Lattice parameters have been automatically calculated by the PDXL software version 1.6.0.1 with the ICDD version 6.0 database. Surface morphologies of the samples were studied by using a Zeiss/Supra 55 Scanning Electron Microscopy (SEM).

Samples with x = 0.25, 0.3, and 0.35 Au contents will hereafter be named A, B, and C, respectively.

## 3 Results and discussion

### 3.1 XRD characterization

Figure 1 shows the powder XRD patterns of all samples. It is obvious that all samples present the Bi-2212 phase as the major one, accompanied by small amounts of secondary phases such as $Bi_2CaO_4$. Moreover, metallic Au can be also identified, implying that Au is not incorporated in the crystal structure of Bi-2212 phase. This fact is confirmed when observing the peaks associated to the Bi-2212 phase, which appear at the same angles. Moreover, the lattice parameters displayed in Table 1 for all samples clearly show that there is no significant difference between them (even considering the data obtained in [24]), further confirming that Au does not enter into the Bi-2212 crystal structure. In fact, the Au behaviour can be related to the observed for metallic Ag, which promotes better grain connectivity by filling the pores between the grains [25].

In addition, it is quite difficult to estimate the grain thickness of a Bi-2212 crystallite due to the fact that they form aggregates with their *ab*-planes parallel to each other. However, it can be correctly calculated using the Debye–Scherrer equation [26]. It is clear from Fig. 1 that the peak intensities and shapes do not significantly change, indicating that grain sizes are very similar in all cases.

Meanwhile, it should not be forgotten that superconducting properties of the bulk ceramics can be not only influenced by the amount of superconducting phase, but also by the presence of weak or strong grain boundaries, grain alignment, etc.

### 3.2 SEM analysis

Representative SEM micrographs taken on the samples surfaces are shown in Fig. 2a–c. As it can be easily observed in the pictures, all samples present randomly oriented plate-like grains, which is the typical situation for classically sintered materials. Moreover, the surface morphology is practically the same, independently of the Au addition, as well as the grains sizes. This fact, together with the data obtained through XRD, clearly indicates that metallic Au do not substitute any cation in the Bi-2212 crystal structure. Similar results were also observed in the previous study, including the effect of the small amount of nano-sized metallic Au addition on Bi-2212 phase [24].

Moreover, the addition of nano-sized elements into the BSCCO system can lead to defect formation within the superconducting grains. When these defects (point defects, dislocations, or secondary phases) have the right size and

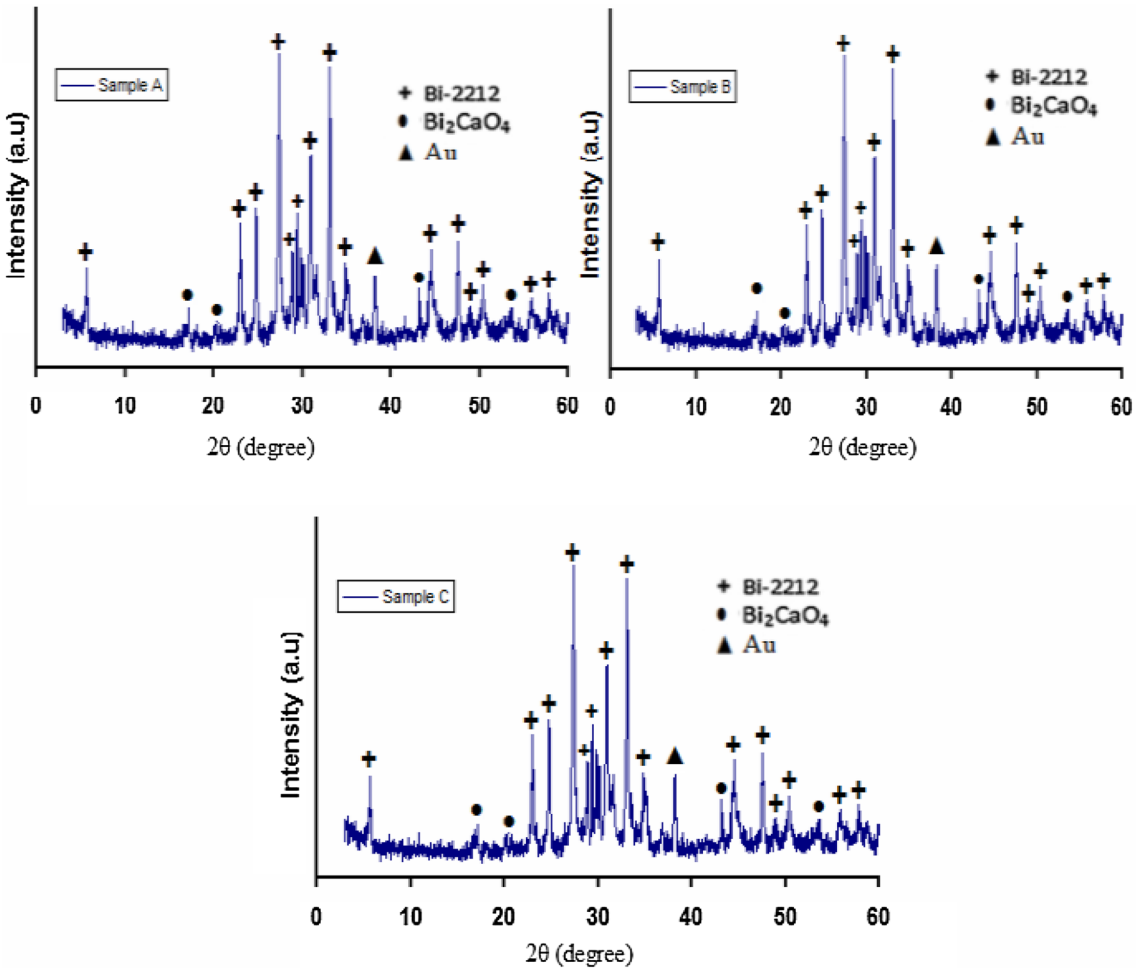


**Fig. 1** XRD patterns of the A, B, and C samples. The symbols indicate the different phases: + Bi-2212; (filled circle) $Bi_2CaO_4$; (filled triangle) Au

**Table 1** Lattice parameters and electrical resistivity values for all samples

| Au contents (x values) | a (Å) | b (Å) | c (Å) | $T_c^{onset}$ (K) | $T_c^{offset}$ (K) | R (mohm-cm) at 150 K |
|---|---|---|---|---|---|---|
| 0.0 | 3.8186* | 3.8186* | 30.833* | 82.2* | 52* | 2.45* |
| 0.05 | 5.4067* | 5.4067* | 30.821* | 79.8* | 52.6* | 1.79* |
| 0.1 | 5.4184* | 5.4184* | 30.868* | 78.4* | 53.9* | 1.64* |
| 0.2 | 5.4076* | 5.4076* | 30.826* | 77.3* | 55.7* | 1.37* |
| 0.25 | 5.4122 | 5.4122 | 30.834 | 76.4 | 58.2 | 1 |
| 0.3 | 5.4128 | 5.4128 | 30.844 | 76.7 | 57.8 | 0.997 |
| 0.35 | 5.4117 | 5.4117 | 30.842 | 76.4 | 57.7 | 0.935 |

As reference, values obtained in lower Au content samples [24] are also included

*The values are taken from previous article

physical characteristics, they can act as effective flux pinning centers leading to higher critical current densities [27–35].

### 3.3 Electrical measurements

Figure 3 shows the electrical resistivity versus temperature curves for all the samples, from 5 to 150 K. As it can be

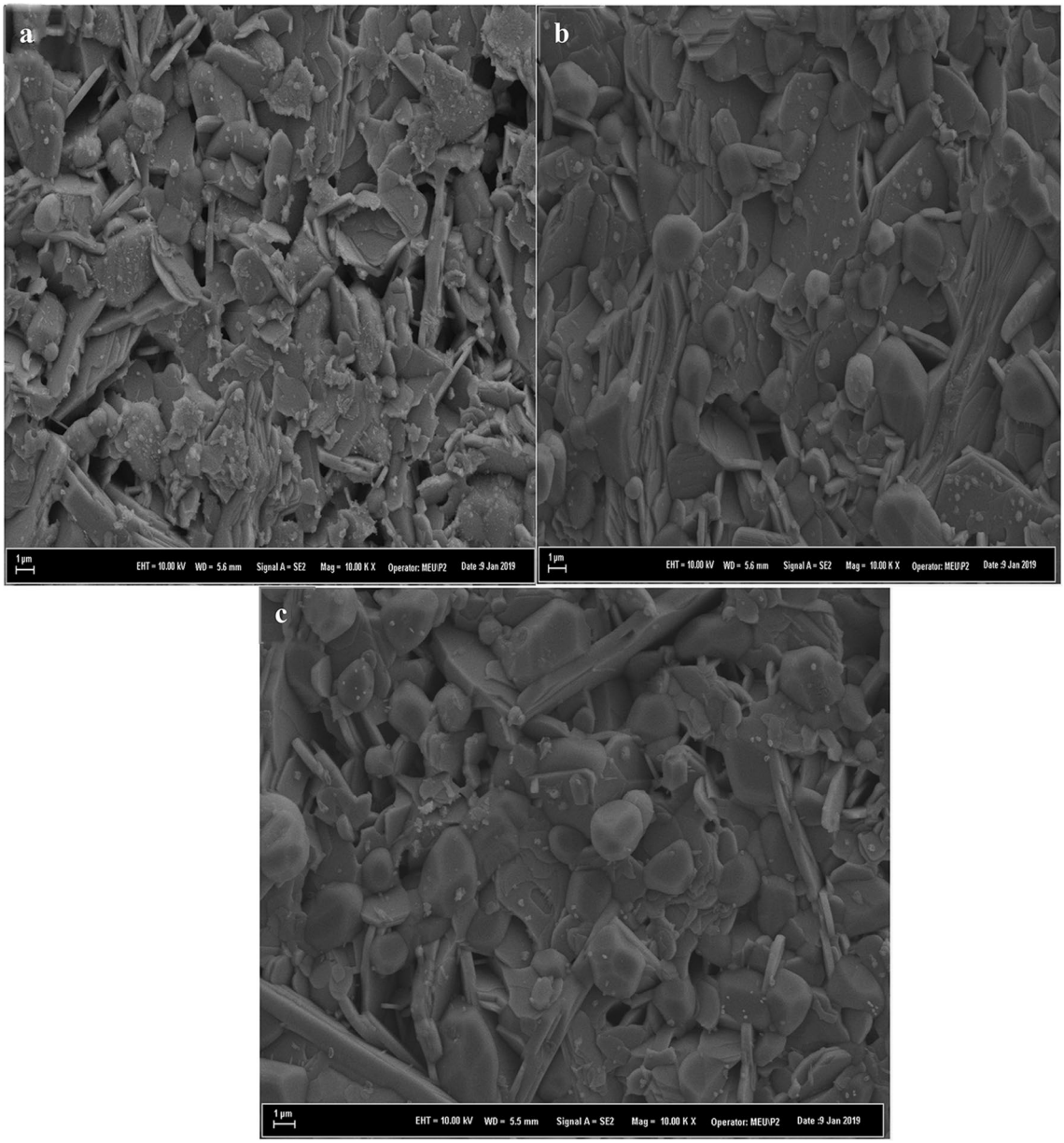


**Fig. 2** SEM micrographs obtained in the surfaces of **a** A; **b** B; and **c** C samples

observed in this graph, all curves show the same behavior in the whole measured temperature range. Moreover, their superconducting transition is quite narrow, between 78 and 60 K, and all samples display metallic characteristics in the normal state, in greement with a low content of Bi-2201 secondary phase. However, in the metallic zone, the electrical resistivity values are very small even at high temperatures, being in fact, slightly lower for sample C in this temperature range. These data can be explained by the large volume fraction of metallic Au in sample C, which can lead to a slight decrease of porosity in the samples, being responsible of its lower resistivity. Furthermore, the effect of these metallic additions are not limited to the electrical properties, as they also influence mechanical properties in agreement with previous works in metal-ceramic composites [36, 37].

The numerical electrical resistivity results of all samples are given in Table 1, together with the results obtained in [24]. When comparing these data, it is very clear that the variation of $T_c$ (offset) values with Au content are negligible. It is probably due to the fact that Au does not incorporate into the Bi-2212 crystal structure.

Actually, it is considered that the adding of nano-particles at high contents can increase the cooper pair breaking rate [38]. However, it is obvious that despite the addition of large

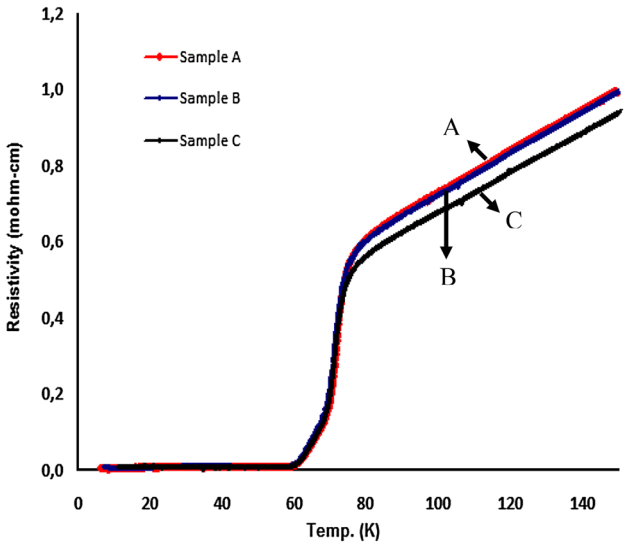


**Fig. 3** Electrical resistivity as a function of temperature curves for the samples

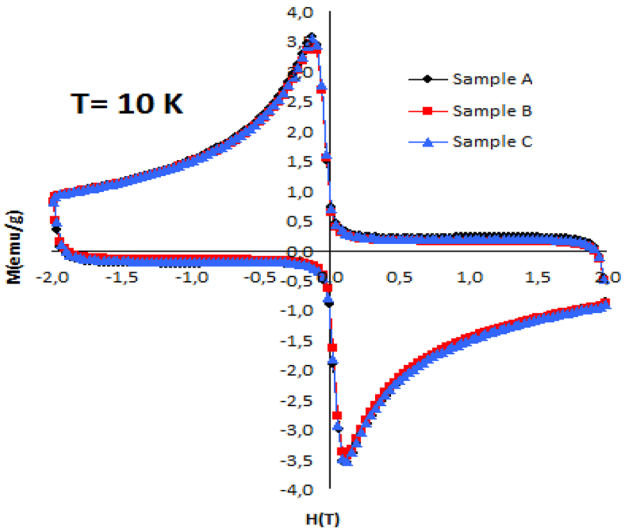


**Fig. 5** Magnetization hysteresis curves for all samples measured at 10 K and ± 2 T external applied magnetic field

amounts of the nano-sized metallic Au into Bi-2212 system, its superconducting properties are not negatively affected. This effect can be also explained taking into account that the charge carrier concentration will be maintained constant, as the Bi-2212 phase composition is not modified by the presence of metallic Au.

### 3.4 Magnetic properties

The magnetic–hysteresis cycles have been measured in all samples, between ± 2 T applied field, at both 2 and 10 K, and are presented in Figs. 4 and 5, respectively. The reason for recording M–H curves at very low temperature (2 K), is because it allows observing the effect produced by nano-sized metallic Au additions. When observing both graphs, it can be observed that small differences between the samples appear at 2 K, while they overlap at 10 K. This behaviour can be explained the very similar nature of all samples with respect to the Bi-2212 phase.

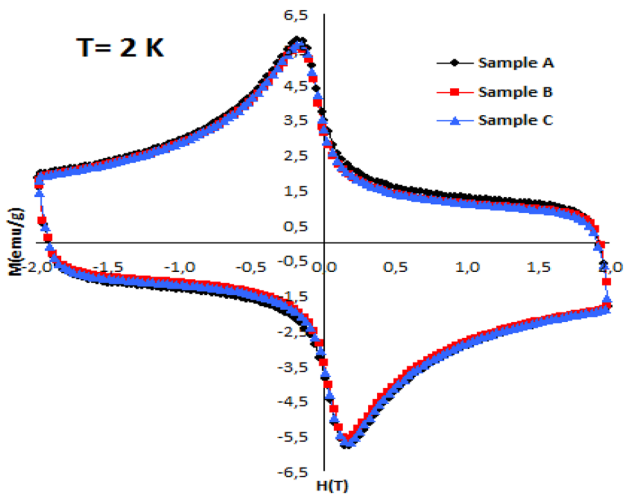


**Fig. 4** Magnetization hysteresis curves for all samples measured at 2 K and ± 2 T external applied magnetic field

As expected, the largest area of the M–H curves has been obtained at 2 K in all samples. In these conditions, it is generally suggested that the dominant effect is the volume fraction of the superconducting phase. At higher magnetic fields and temperatures, the changes in M–H curves strongly depend on flux pinning properties and the strong-links between the grains [39]. It can be clearly seen in Fig. 5 that no significant differences in magnetization values are produced, indicating that the diamagnetic character of the Bi-2212 phase is not affected by Au, in spite of the remarkable changes observed in the I–V curves. This difference is due to the fact that I–V behaviour reflects microstructural effects such as defects, voids and conductivity between grains. Moreover, the presence of metallic Au can contribute to the intergrain electrical conductivity [40], while it is not affecting the diamagnetic response due to its non magnetic nature.

The $J_C$ values of the samples were calculated at both 2 and 10 K, using the Bean's model [41, 42]:

$$\mathrm{Jc} = 20\frac{\Delta M}{a\left(1-\frac{a}{3b}\right)}$$

where $J_c$ is the magnetization current density in ampèresper square centimeter of a sample. $\Delta M = M_+ - M_-$ is measured in electromagnetic units per cubic centimeter, a and b ($a < b$)

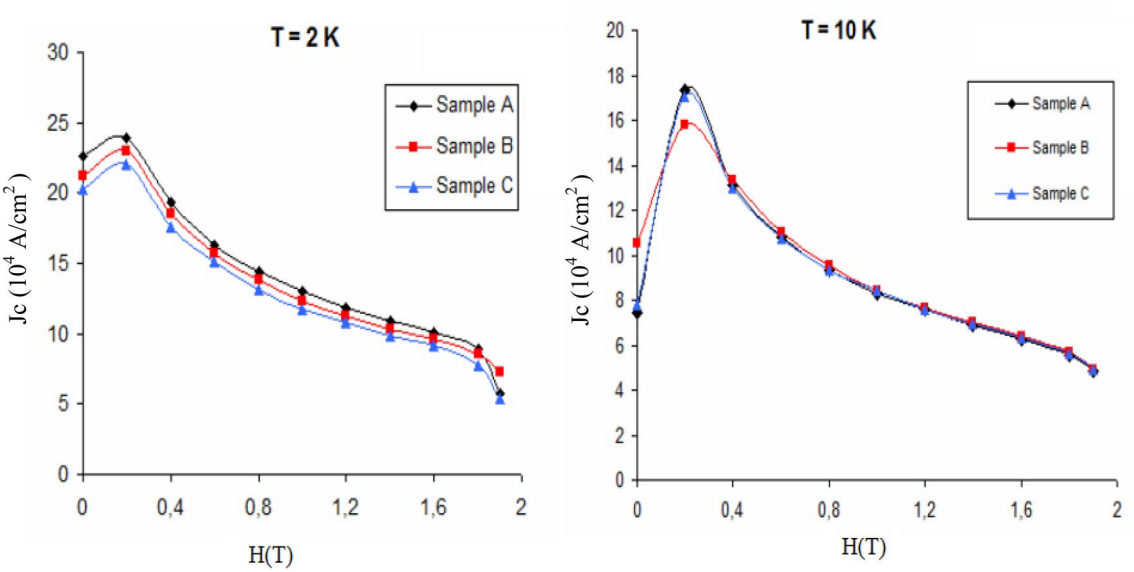


**Fig. 6** Calculated critical current densities for all the samples at both 2 and 10 K as a function of the applied field

are the dimensions in centimeters of the crosssection of the sample parallel to the applied field. It is important to note that the $J_c$ values calculated in this study mainly reflect intragrain $J_c$, which are usually larger than the real ones obtained by direct measurements which are influenced by the presence of weak links and other type of defects [2, 42–44].

Figure 6 shows $J_c$ values for all the samples at both 2 and 10 K. It is obvious that even if the $J_c$ values of all samples including the additions of nano-sized metallic Au in high contents prepared in this study are close to each other, they are higher than the reported in samples with low Au content [24]. The highest values at 2, and 10 K have been obtained in sample A (about $2.5 \times 10^5$, and $1.8 \times 10^5$, respectively), which are lower than the obtained in samples prepared through more complicated methods ($2 \times 10^6$ A/cm$^2$ at 20 K [22]).

## 4 Conclusions

$Bi_{1.8}Sr_2Au_xCa_{1.1}Cu_{2.1}O_y$ superconductors with Au nanoparticles addition, and x ranging from 0.25 to 0.35, were synthesized by conventional the solid-state method. All the preparation parameters such as grinding time, sintering temperature, pressing pressure, etc., used in this study were the same reported in a previous work, in which Au content is in the range of x = 0.0–0.2. Powder XRD patterns clearly show that there is no noticeable difference in the positions and intensities of the Bi-2212 phase diffraction peaks, meaning that Au does not influence the Bi-2212 phase formation. The critical transition temperatures obtained in this study are higher than samples with small amounts of Au content, possibly due to the formation of better intergrain connectivity induced by metallic Au. Moreover, the width of M–H loops of all samples are wider than the ones presented in samples with lower Au content, showing the improvement of the superconducting properties of Bi-2212 phase. The highest $J_c$ value ($4.9 \times 10^4$ A/cm$^2$) under 1.9 T applied magnetic field have been obtained for 0.3 Au added sample at 10 K, while for the pure sample it was $2.1 \times 10^4$ A/cm$^2$ at the same temperature and magnetic field.

**Acknowledgements** This work is supported by the BAP Research Fund of Mersin University, Mersin, Turkey, under Grant Contracts No: 2016-2-TP2-1849. All samples have been prepared in the Energy Laboratory in Tarsus University in Turkey. Both SEM and XRD measurements have been made in the MEİTAM Central Laboratory in Mersin University. Other measurements in this study have been made in the METU Central Laboratory in Middle East Technical University in Ankara in Turkey. On the other hand, I wish to thank M.Sc. Aynur GURBÜZ and M.Sc. Seher KURU in the MEİTAM Central Laboratory and Dr. Ibrahim ÇAM in the METU Central Laboratory for their experimental support and very meticulous work.

## References

1. T. Che, Y.F. Gou, J. Zheng, R.X. Sun, D.B. He, Z.G. Deng, J. Supercond. Nov. Magn. **27**, 2211 (2014)
2. U. Topal, M.E. Yakinci, Mater. Chem. Phys. **119**, 182 (2010)
3. G. Krabbes, G. Fuchs, P. Verges, P. Diko, G. Stover, S. Gruss, Physica C **636**, 378 (2002)
4. U. Topal, F. Alikma, C. Birlikseven, J. Supercond. Nov. Magn. **25**, 931 (2012)
5. T. Masuda, T. Kato, H. Yumura, M. Watanabe, Y. Ashibe, K. Ohkura, C. Suzawa, M. Hirose, S. Isojima, K. Matsuo, S. Honjo, T. Mimura, T. Kuramochi, Y. Takahashi, H. Suzuki, T. Okamoto, Physica C **1174**, 378 (2002)

6. H. Maeda, Y. Tanaka, M. Fukutumi, T. Asano, Jpn. J. Appl. Phys. **27**, L209–L210 (1988)
7. S.E.M. Ghahfarokhi, M.Z. Shoushtari, Phys. Rev. B: Condens. Matter **405**, 4643 (2010)
8. Y. Huang, G.F. de la Fuente, A. Sotelo, A. Badia, F. Lera, R. Navarro, C. Rillo, R. Ibanez, D. Beltran, F. Sapina, A. Beltran, Physica C **185**, 2401 (1991)
9. O. Nane, B. Ozcelik, M.A. Madre, A. Sotelo, J. Eur. Ceram. Soc. **37**, 1007 (2017)
10. F. Kahraman, A. Sotelo, M.A. Madre, J.C. Diez, B. Ozkurt, Sh Rasekh, Ceram. Int. **41**, 14924 (2015)
11. B. Özkurt, M.A. Madre, A. Sotelo, J.C. Diez, Physica B Condens. Matter. **426**, 85 (2013)
12. M.E. Aytekin, B. Özkurt, İ. Sugözü, J. Mater. Sci.: Mater. Electron. **26**, 1799 (2015)
13. M.E. Aytekin, B. Özkurt, K.B. Sugözü, E. Köse, İ. Sugözü, J. Mater. Sci. **27**, 8068 (2016)
14. B. Özkurt, M.A. Madre, A. Sotelo, J.C. Diez, J. Mater. Sci.: Mater. Electron. **24**, 3344 (2013)
15. A. Sotelo, B. Ozcelik, H. Amaveda, A. Bruned, M.A. Madre, Ceram. Int. **41**, 14276 (2015)
16. S.H. Lee, Mater. Chem. Phys. **75**, 166 (2002)
17. B. Özkurt, M.A. Madre, A. Sotelo, M.E. Yakıncı, B. Özçelik, J.C. Diez, J. Supercond. Nov. Magn. **26**, 1093 (2013)
18. B. Özçelik, B. Özkurt, M.E. Yakıncı, A. Sotelo, M.A. Madre, J. Supercond. Nov. Magn. **26**, 873 (2013)
19. V. Lennikov, B. Özkurt, L.A. Angurel, A. Sotelo, B. Özçelik, G.F. de la Fuente, J. Supercond. Nov. Magn. **26**, 947 (2013)
20. B. Ozkurt, J. Mater. Sci. **24**, 2426 (2013)
21. O. Nane, B. Özçelik, H. Amaveda, A. Sotelo, M.A. Madre, Ceram. Int. **42**, 8473 (2016)
22. N. Chikumoto, K. Furusawa, M. Murakami, Physica C **412**, 463 (2004)
23. F.M. Costa, N.M. Ferreira, Sh Rasekh, A.J.S. Fernandes, M.A. Torres, M.A. Madre, J.C. Diez, A. Sotelo, Cryst. Growth Des. **15**, 2094 (2015)
24. Ugur Öztornacı, Berdan Özkurt, Ceram. Int. **43**, 4545 (2017)
25. F.M. Costa, Sh Rasekh, N.M. Ferreira, A. Sotelo, J.C. Diez, M.A. Madre, J. Supercond. Nov. Magn. **26**, 943 (2013)
26. A. Taylor, H. Sinclair, Proc. Phys. Soc. **57**, 126 (1945)
27. M. Roumie, S. Marhaba, R. Awad, M. Kork, I. Hassan, R. Mawassi, J. Supercond. Nov. Magn. **27**, 143 (2014)
28. M. Annabi, A. M'chirgui, F.B. Azzouz, M. Zouaoui, M.B. Salem, Physica C **405**, 25 (2004)
29. X. Wan, Y. Sun, W. Song, K. Wang, L. Jiang, J. Du, Physica C **307**, 46 (1998)
30. M. Däumling, J.C. Grivel, B. Hensel, R. Flükiger, Physica C **219**, 429 (1994)
31. P.E. Kazin, M. Jansen, A. Larrea, G.F. de la Fuente, YuD Tretyakov, Physica C **253**, 391 (1995)
32. B.A. Albiss, I.M. Obaidat, M. Gharaibeh, H. Ghamlouche, S.M. Obeidat, Solid State Commun. **150**, 1542 (2010)
33. T. Çördük, Ö. Bilgili, K. Kocabaş, J. Mater. Sci. **28**, 14689 (2017)
34. A.I. Abou-Aly, M.A. Gawad, R. Awad, I. G-Eldeen, J. Supercond. Nov. Magn. **24**, 2077 (2011)
35. A. Ghattas, M. Annabi, M. Zouaoui, F.B. Azzouz, M.B. Salem, Physica C **468**, 31 (2008)
36. S. Celik, O. Ozturk, E. Coşkun, M. Sarıhan, E. Aşikuzun, K. Ozturk, C. Terzioglu, J. Mater. Sci. **24**, 2218 (2013)
37. F. Kahraman, M.A. Madre, Sh Rasekh, C. Salvador, P. Bosque, M.A. Torres, J.C. Diez, A. Sotelo, J. Eur. Ceram. Soc. **35**, 3835 (2015)
38. H.K. Barik, S.K. Ghorai, S. Bhattacharya, D. Kilian, B.K. Chaudhuri, J. Mater. Res. **15**, 1076 (2000)
39. D.C. van der Laan, H.J.N. van Eck, B. Ten Haken, J. Schwartz, H.H.J. ten Kate, IEEE Trans. Appl. Supercond. **11**, 3345 (2001)
40. M. Ruano, M. Diaz, L. Martinez, E. Navarro, E. Roman, M. Garcia-Hernandez, A. Espinosa, C. Ballesteros, R. Fermento, Y. Huttel, Phys. Chem. Chem. Phys. **15**, 316 (2013)
41. C.P. Bean, Phys. Rev. Lett. **8**, 250 (1962)
42. I.B. Bobylev, E.G. Gerasimov, N.A. Zyuzeva, Phys. Solid State **54**, 1633 (2012)
43. B. Özkurt, J. Alloys Compd. **579**, 132 (2013)
44. Z.Y. Jia, H. Tang, Z.Q. Yang, Y.T. Xing, Y.Z. Wang, G.W. Qiao, Physica C **337**, 130 (2000)